Liquid Crystals
Publication details, including instructions for authors and subscription information:
http://www.informaworld.com/smpp/title~content=t713926090

Lyotropic mesomorphism of alkyl esters of acyl-L-carnitines

Paolo De Maria[a]; Sara Frascari[b]; Paolo Mariani[c]; Letizia Saturni[c]; Gian Piero Spada[b]; Maria Ornella Tinti[d]
[a] Facoltà di Farmacia, Università di Chieti, Chieti, Italy [b] Dipartimento di Chimica Organica 'A. Mangini', Università di Bologna, Bologna, Italy [c] Istituto di Scienze Fisiche, Facoltà di Medicina, Università di Ancona, Italy [d] Sigma Tau S.p.A., Dipartimento Ricerche Chimiche, Italy

To cite this Article De Maria, Paolo , Frascari, Sara , Mariani, Paolo , Saturni, Letizia , Spada, Gian Piero and Tinti, Maria Ornella(1995) 'Lyotropic mesomorphism of alkyl esters of acyl-L-carnitines', Liquid Crystals, 19: 3, 353 — 365
To link to this Article: DOI: 10.1080/02678299508031992
URL: http://dx.doi.org/10.1080/02678299508031992

LIQUID CRYSTALS, 1995, VOL. 19, NO. 3, 353–365

Lyotropic mesomorphism of alkyl esters of acyl-L-carnitines

by PAOLO DE MARIA†, SARA FRASCARI‡, PAOLO MARIANI§*, LETIZIA SATURNI§, GIAN PIERO SPADA‡ and MARIA ORNELLA TINTI¶

† Facoltà di Farmacia, Università di Chieti, via dei Vestini 30, 66013 Chieti, Italy
‡ Dipartimento di Chimica Organica 'A. Mangini', Università di Bologna, via S. Donato 15, 40127 Bologna, Italy
§ Istituto di Scienze Fisiche, Facoltà di Medicina, Università di Ancona, via Ranieri 65, 60131 Ancona and INFM, unità di Ancona, Italy
¶ Sigma Tau S.p.A., Dipartimento Ricerche Chimiche, via Pontina Km 30.400, 00040 Pomezia (Roma), Italy

(*Received 28 November 1995; in final form 2 February 1995; accepted 20 March 1995*)

The lyotropic polymorphism of a series of alkyl esters of acyl-L-carnitine has been studied by optical polarizing microscopy and X-ray diffraction. The different structures observed as a function of concentration and temperature have been characterized and their topology determined. As a result, two different phase sequence patterns have been detected: esters of normal alcohols bearing an alkyl chain of 6 or more carbon atoms in the acyl substituent display only a lamellar phase, while compounds which bear a relatively short alkyl chain (4 or less carbon atoms) show in addition non-lamellar type I hexagonal and cubic Q^{230} phases. From the analysis of the areas-per-molecule at the polar/apolar interface, the ability of the compounds investigated to form not only non-lamellar phases, but also direct micelles in isotropic solution has been related to the structural characteristics of the molecules. Curved, convex interfaces (in micelles and in non-lamellar phases) are possible only for the most polar acylcarnitines which have a relatively short alkyl chain, so that they behave like single chain surfactants; the most paraffinic derivatives, which have a relatively long alkyl chain, are effective double chain surfactants and then generate only quasi-planar interfaces.

1. Introduction

L-carnitine [(*R*)-3-hydroxy-4-trimethylammoniumbutanoate] is a necessary cofactor for the transport of fatty acids across the inner mitochondrial membrane [1]. There is convincing evidence [2] that a carnitine–acylcarnitine translocase in the inner membrane is responsible for the coupled influx and efflux of these molecules. These acylcarnitines are amphiphilic and resemble in some structural respects lysolecithins; in fact it was shown [3] by X-ray diffraction studies that palmitoyl-L-carnitine at low temperature forms a gel-phase bilayer and as the temperature is increased a transition occurs to a type I hexagonal phase. It is also known [4] that standard solutions cannot be prepared in water because, even at below critical micelle concentration, palmitoyl-L-carnitine does not distribute uniformly in solution. This compound is very surface active and prefers to leave the bulk phase to segregate at the water/air or water/apolar interphase. In consideration of our interest [5] in carnitines and of the promising supramolecular properties [2–4] of palmitoyl-L-carnitine, we thought it interesting to investigate by optical microscopy and X-ray diffraction the different mesophases formed at above critical micelle concentration by the long chain acylcarnitine esters reported in the chart.

The compounds chosen have been proved to possess antimicrobial activity, particularly towards gram-positive bacteria and filamentous fungii (including *dermatophytes*), and the biological activity apparently depends upon the length of the alkyl chains present in the ester groups of the carnitine.

* Author for correspondence.

2. Experimental

2.1. *Materials*

Acyl-L-carnitines were prepared according to [6]. Long chain alcohols from Aldrich were used without additional purification.

0267–8292/95 $10·00

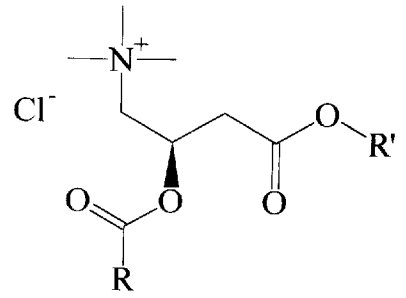

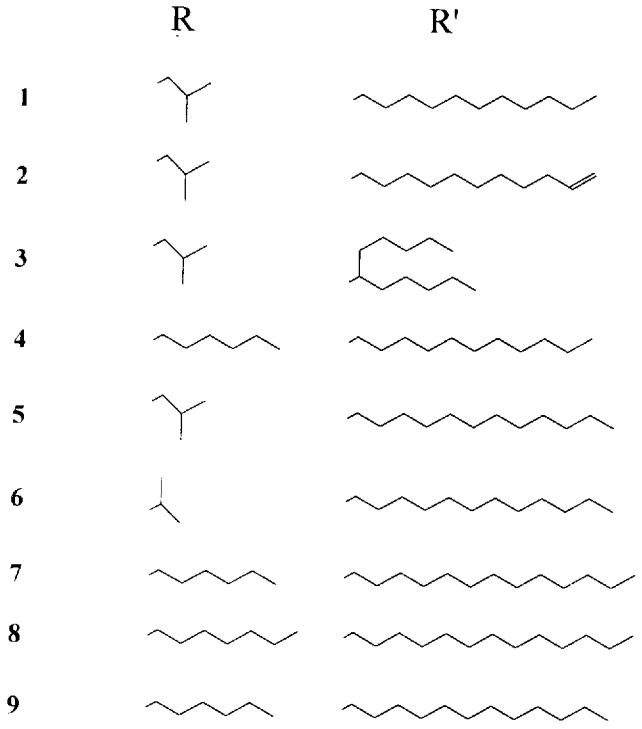

2.1.1. *General procedure for the synthesis of compounds* **1–9**

The acyl-L-carnitine chloride (0·1 mol) was suspended in dry methylene chloride (100 ml). The mixture was cooled to 0°C and oxalyl chloride (13 ml, 0·15 mol) in anhydrous CH_2Cl_2 (15 ml) was slowly added with stirring. After 30 min at room temperature, a further amount of oxalyl chloride (19 ml, 0·21 mol) in anhydrous CH_2Cl_2 (10 ml) was added. The resulting solution was left stirring for 2 h at room temperature, then concentrated under reduced pressure. The residue thus obtained was washed twice with anhydrous CH_2Cl_2 and concentrated under reduced pressure. The raw acyl chloride thus obtained was used as such in the next reaction. The acyl chloride (0·1 mol) was dissolved in anhydrous CH_2Cl_2 (40 ml). The solution was cooled to 0°C and the appropriate long chain alcohol (0·168 mol) in CH_2Cl_2 (35 ml) was added under a nitrogen atmosphere. The solution was then stirred at room temperature for 2 h and finally concentrated under reduced pressure until an oily residue was obtained. The raw reaction mixture was chromatographed on a silica gel column buffered with 2 per cent Na_2HPO_4. CH_2Cl_2 was used as eluent for residual long chain alcohol, and then CH_2Cl_2/MeOH (9 : 1) for complete elution of the desired compound. The pooled fractions were concentrated and gave the following acyl-L-carnitine esters.

2.1.2. *Characterization of the compounds*

Isovaleryl-L-carnitine undecyl ester chloride, **1**. $[\alpha]_D^{25} = -10{\cdot}5$ ($c = 1$ per cent H_2O). Analysis calculated for $C_{23}H_{46}ClNO_4$: C, 63·35; H, 10·63; Cl, 8·13; N, 3·21. Found: C, 60·87; H, 10·88; Cl, 8·14; N, 3·29; H_2O 2·4 per cent. HPLC Column: Spherisorb Cl (5 μm) 200 mm, i.d. 4·6 mm. $T = 50$°C. Mobile phase: CH_3OH/KH_2PO_4 50 mM (65 : 35). Flow rate: 1 ml min^{-1}. Rt: 14·82 min. δ_H ($CDCl_3$) 5·5 (1 H, m, –CH–), 4·2–3·8 (4 H, m, N^+CH_2; OCH_2), 3·3 (9 H, s, $(CH_3)_3N^+$), 2·8 (2 H, m, CH_2COO), 2·2 (2 H, m, $OCOCH_2$), 1·6–1·0 (22 H, m, C<u>H</u> $(CH_3)_2$, $(CH_2)_9CH_3$), 0·8 (6 H, d, $CH(C\underline{H}_3)_2$; m.p. not determined (hygroscopic).

Isovaleryl-L-carnitine undec-10-enyl ester chloride, **2**. $[\alpha]_D^{25} = -11{\cdot}1$ ($c = 1$ per cent $CHCl_3$). Analysis calculated for $C_{23}H_{44}NO_4Cl$: C, 63·64; H, 10·22; Cl, 8·17; N, 3·23. Found: C, 61·43; H, 10·66; Cl, 7·40; N, 3·14; H_2O 1·5 per cent. HPLC Column: Nucleosil-SA (5 μm) 200 mm, i.d. 4·0 mm. $T = 40$°C. Mobile phase: $(NH_4)_2HPO_4$ 50 mM/CH_3CN 1 : 1 pH 4 with H_3PO_4. Flow rate: 0·75 ml min^{-1}. Rt: 14·92 min. δ_H (CD_3OD) 6·0–5·8 (1 H, m, $CH{=}CH_2$), 5·7 (1 H, m, CHOCO), 5·1–5·0 (2 H, m, $CH{=}C\underline{H}_2$), 4·2 (2 H, t, $COOCH_2$), 4·0–3·8 (2 H, m, N^+CH_2), 3·3 (9 H, s, $(CH_3)_3N^+$), 2·9 (2 H, m, CH_2COO), 2·3 (2 H, d, $OCOCH_2$), 2·2–2·0 (3 H, m, CH_2, C<u>H</u>$(CH_3)_2$), 1·7 (2 H, m, CH_2), 1·4 (14 H, broad, $7CH_2$), 1·0 (6 H, d, $2CH_3$); m.p. not determined (oil).

Isovaleryl-L-carnitine 1-pentylhexyl ester chloride, **3**. $[\alpha]_D^{25} = -12{\cdot}9$ ($c = 1$ per cent H_2O). Analysis calculated for $C_{23}H_{46}NO_4Cl$: C, 63·35; H, 10·63; Cl, 8·13; N, 3·21. Found: C, 61·33; H, 10·81; Cl, 6·69; N, 3·27; H_2O 1·3 per cent. HPLC Column: Spherisorb-C1 (5 μm) 200 mm, i.d. 4·6 mm. $T = 40$°C. Mobile phase: CH_3OH/KH_2PO_4 50 mM 65 : 35 pH 4·5 with H_3PO_4. Flow rate: 1 ml min^{-1}. Rt: 7·39 min. δ_H ($CDCl_3$) 5·7 (2 H, m, CHO), 4·8 (1 H, q, CH); 4·4–4·0 (2 H, m, N^+CH_2), 3·4 (9 H, s, $N^+(CH_3)_3$), 2·8 (2 H, m, CH_2COO), 2·2 (2 H, m, $OCOCH_2$), 2·1 (1 H, m, C<u>H</u>$(CH_3)_2$), 1·5 (4 H, m, $2CH_2$), 1·3 (6 H, broad, $3CH_2$), 1·0–0·9 (9 H, d + t, $CH(C\underline{H}_3)_2$, CH_3); m.p. 150–160°C (decomp).

Heptanoyl-L-carnitine undecyl ester chloride, **4**. $[\alpha]_D^{25} = -12{\cdot}1$ ($c = 1$ per cent H_2O). Analysis calculated for $C_{25}H_{49}NO_4Cl$: C, 64·69; H, 10·86; Cl, 7·64; N, 3·02. Found: C, 64·35; H, 12·55; C1, 6·68; N, 3·09; H_2O 1·3 per cent. HPLC Column: Spherisorb-Cl (5 μm) 200 mm,

i.d. 4·6 mm. $T = 40°C$. Mobile phase: CH_3OH/KH_2PO_4 50 mM 65:35 pH 4·5 with H_3PO_4. Flow rate: 0·5 ml min^{-1}. Rt: 9·35 min. δ_H (D_2O) 5·7 (1 H, m, CHO), 4·1 (2 H, t, OCH_2), 4·0–3·7 (2 H, m, CH_2N^+), 3·2 (9 H, s, $(CH_3)_3N^+$), 3·0–2·7 (2 H, m, CH_2COO); 2·5–2·3 (2 H, m, $COCH_2$), 1·6 (4 H, m, $2CH_2$), 1·3 (22 H, m, $11CH_2$), 0·9–0·8 (6 H, 2t, $2CH_3$); m.p. not determined.

Isovaleryl-L-carnitine dodecyl ester chloride, **5**. $[\alpha]_D^{25} = -12·2$ ($c = 1$ per cent H_2O). Analysis calculated for $C_{24}H_{48}NO_4Cl$: C, 64·04; H, 10·75; Cl, 7·88; N, 3·11. Found: C, 63·46; H, 12·26; Cl 7·81; N, 3·15; H_2O 1·0 per cent. HPLC Column: Nucleosil-SA (5 μm) 200 mm, i.d. 4·0 mm. $T = 40°C$. Mobile phase: $(NH_4)_2HPO_4$ 50 mM/CH_3CN 1:1 pH 4 with H_3PO_4. Flow rate: 0·75 ml min^{-1}. Rt: 12·65 min. δ_H ($CDCl_3$) 5·7 (1 H, m, CHO), 4·4–4·0 (4 H, m, N^+CH_2; OCH_2), 3·5 (9 H, s, $N^+(CH_3)_3$), 2·8 (2 H, m, CH_2COO), 2·2 (2 H, m, $OCOCH_2$), 2·0 (1 H, m, $C\underline{H}(CH_3)_2$), 1·6 (2 H, m, CH_2), 1·2 (18 H, broad, $9(CH_2)$), 0·9–0·8 (9 H, d + t, CH_3, $(CH_3)_2$); m.p. 150–160°C (decomp).

Isobutyryl-L-carnitine dodecyl ester chloride, **6**. $[\alpha]_D^{25} = -14·5$ ($c = 1$ per cent H_2O). Analysis calculated for $C_{23}H_{46}NO_4Cl$: C, 63·35; H, 10·63; Cl, 8·13; N, 3·21. Found: C, 62·90; H, 11·47; Cl, 7·86; N, 3·27; H_2O 0·4 per cent. HPLC Column: Nucleosil-SA (5 μm) 1·2 mm, i.d. 4·0 mm. $T = 40°C$. Mobile phase: $(NH_4)_2HPO_4$ 50 mM/CH_3CN 1:1 pH 4 with H_3PO_4. Flow rate: 0·75 ml min^{-1}. Rt: 14·0 min. δ_H ($CDCl_3$) 5·7 (1 H, m, CHO), 4·4–4·0 (4 H, m, N^+CH_2; OCH_2), 3·5 (9 H, s, $N^+(CH_3)_3$), 2·9–2·7 (2 H, m, CH_2COO), 2·6–2·5 (1 H, m, $C\underline{H}(CH_3)_2$), 1·6 (2 H, m, CH_2), 1·3 (18 H, broad, $9CH_2$), 1·1 (6 H, d, $CH(CH_3)_2$, 0·8 (3 H, t, CH_3); m.p. 150–155°C (decomp).

Heptanoyl-L-carnitine tridecyl ester chloride, **7**. $[\alpha]_D^{25} = -10·3$ ($c = 0·7$ per cent $CHCl_3$). Analysis calculated for $C_{27}H_{54}NO_4Cl$: C, 65·89; H, 11·06; Cl 7·20; N, 2·85. Found: C, 65·26; H, 11·62; Cl, 6·70; N, 2·87; H_2O 0·3 per cent. HPLC Column: Nucleosil-SA (5 μm) 200 mm, i.d. 4·0 mm, $T = 30°C$. Mobile phase: $(NH_4)_2HPO_4$ 50 mM/CH_3CN 65:35 pH 3·5 with H_3PO_4. Flow rate: 0·75 ml min^{-1}. Rt: 9·13 min. δ_H ($CDCl_3$) 5·7 (1 H, m, CHO), 4·3–4·0 (4 H, m, CH_2N^+, OCH_2), 3·5 (9 H, s, $(CH_3)_3N^+$), 2·8 (2 H, m, CH_2COO), 2·3 (2 H, m, $OCOCH_2$), 1·6 (4 H, m, $2CH_2$), 1·3 (26 H, m, $13CH_2$), 0·9 (6 H, 2t, $2CH_3$); m.p. 150–160°C (decomp).

Octanoyl-L-carnitine tridecyl ester chloride, **8**. $[\alpha]_D^{25} = -9·8$ ($c = 1$ per cent $CHCl_3$). Analysis calculated for $C_{28}H_{56}NO_4Cl$: C, 66·43; H, 11·15; Cl, 7·00; N, 2·77. Found: C, 66·46; H, 11·93; Cl, 6·93; N, 2·71; H_2O 0·7 per cent. HPLC Column: Spherisorb-Cl (5 μm) 200 mm, i.d. 4·6 mm. $T = 50°C$. Mobile phase: CH_3OH/KH_2PO_4 50 mM 70:30 pH 3·9 with H_3PO_4. Flow rate: 0·5 ml min^{-1}. Rt: 14·71 min. δ_H ($CDCl_3$) 5·7 (1 H, m, CHO), 4·3–4·0 (4 H, m, CH_2N^+, OCH_2), 3·5 (9 H, s $(CH_3)_3N^+$), 2·9–2·7 (2 H, m, CH_2COO), 2·3 (2 H, m, $OCOCH_2$), 1·6 (4 H, m, $2CH_2$), 1·3 (28 H, broad, $14CH_2$), 0·9 (6 H, m, $2CH_3$); m.p. 150–160°C (decomp).

Heptanoyl-L-carnitine dodecyl ester chloride, **9**. $[\alpha]_D^{25} = -12·7$ ($c = 1$ per cent CH_3OH). Analysis calculated for $C_{26}H_{52}NO_4Cl$: C, 65·31; H, 10·96; Cl, 7·41; N, 2·93. Found: C, 67·00; H, 12·12; Cl, 6·60; N, 2·41; H_2O 0·6 per cent. HPLC Column: Spherisorb-Cl (5 μm) 200 mm, i.d. 4·6 mm. $T = 40°C$. Mobile phase: CH_3OH/KH_2PO_4 50 mM 65:35 pH 4·5 with H_3PO_4. Flow rate: 1 ml min^{-1}. Rt: 10·47 min. δ_H ($CDCl_3$) 5·7 (1 H, m, CHO), 4·4–4·0 (4 H, m, N^+CH_2, OCH_2), 3·5 (9 H, s, $N^+(CH_3)_3$), 2·8 (2 H, m, CH_2COO), 2·4 (2 H, t, $COOCH_2$), 1·6 (2 H, m, $2CH_2$), 1·3 (26 H, broad, $13CH_2$), 0·9 (6 H, 2t, $2CH_3$); m.p. not determined.

NMR spectra were recorded with a Varian VXR 300 MHz spectrometer. NMR data are reported with tetramethylsilane as the reference. Optical rotations were measured with a Perkin–Elmer 241 MC polarimeter. HPLC chromatograms were obtained with a Waters chromatograph: pump 600 MS, injection autosample 715, detector UV 484, $\lambda = 205$ nm, R.I. 410 (Software Millenium). Melting points were measured with a Mettler FP 80 apparatus. The water content was measured with a Mettler DL 18 Karl Fischer Titrator following the US Pharmacopea XII edition.

2.1.3. *Molecular volumes*

In order to derive the structural parameters, the volume of the paraffinic residues for the different compounds has been calculated: in particular, as reported in [7] and as typically used for liquid crystalline liquid systems [8], the volumes of the CH_3, CH_2 and CH groups in the disordered α-conformation (see below) have been assumed to be 54, 27 and 20·5 $Å^3$, respectively. The volume of the polar head group has been estimated from molecular modelling to be 190 $Å^3$. The resulting specific volumes were all about 1 $cm^3 g^{-1}$.

2.2. *Optical microscopy*

Microscopic observations on samples obtained by peripheral evaporation were carried out with a Zeiss polarizing microscope equipped with a photocamera.

2.3. *X-ray diffraction*

X-ray diffraction measurements were performed using a 1·5 kW Ital-Structures X-ray generator equipped with a Guinier-type focusing camera operating under vacuum; a bent quartz crystal monochromator was used to select the $CuK_{\alpha 1}$ radiation ($\lambda = 1·54$ Å). The diffraction patterns were recorded on a stack of three Kodak DEF-392 films. Samples were held in a vacuum tight cylindrical cell provided with thin mica windows. The cell temperature was controlled with an accuracy of 1°C. To reduce the spottiness arising from possible macroscopic mono-

domains, the cells were continuously rotated during the exposure.

Samples for X-ray diffraction experiments were obtained by mixing controlled amounts of the acylcarnitine ester with freshly double distilled water. The mixtures were left at room temperature until equilibrium conditions were reached (usually in 24 h). Thereafter, the X-ray diffraction spectra were found to be time-independent for periods of 1–2 weeks. The concentration c is expressed in weight of solute per weight of solution. The relative uncertainty of the concentrations was estimated to be 5 per cent.

3. Results

3.1. *Optical microscopy*

Optical microscopy investigations were carried out on samples with a concentration gradient obtained by peripheral evaporation of aqueous solutions. In particular, two typical texture sequence patterns were obtained. In figure 1 a sample is shown for compound **1**: from the centre towards the periphery (i.e. increasing the concentration), an isotropic texture relating to the dilute isotropic solution I, a herring bone texture typical of a hexagonal phase H, a second isotropic texture, which indicates the presence of a second optically isotropic phase labelled I′, and finally a weakly birefringent texture characteristic of a lamellar phase L can be observed. Compounds **2**, **5** and **6** exhibit this same sequence. Therefore, for these compounds (**1**, **2**, **5** and **6**) the following phase sequence has been deduced: I–H–I′–L.

A different pattern is displayed by compounds **3**, **4**, **7**, **8** and **9**: these acylcarnitines show, as a function of concentration, the isotropic texture relating to the dilute isotropic solution I, followed only by the weakly birefringent texture typical of a lamellar phase. The phase sequence for these compounds (**3**, **4**, **7**, **8** and **9**) is then: I–L.

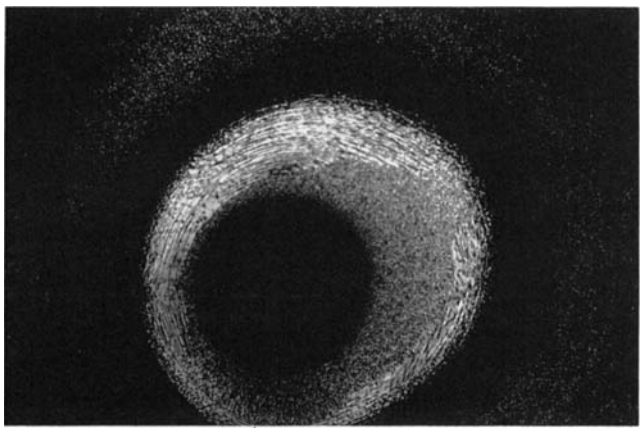

Figure 1. Textures obtained by peripheral evaporation of an aqueous solution of **1**. Concentration increases from the centre towards the periphery; the corresponding phase sequence is I–H–I′–L.

3.2. *X-ray diffraction analysis: phase diagrams*

In order to confirm the nature of the different phases qualitatively observed by optical microscopy and to obtain structural information about the molecular packing and conformations, compounds **1**, **4**–**7** and **9** were investigated as a function of concentration and temperature by X-ray diffraction.

In agreement with the optical microscopy observations, at least three different lyotropic mesophases were identified by X-ray diffraction: these phases display one-parameter structures and belong to one-dimensional (1-D) lamellar (L), two-dimensional (2-D) hexagonal (H) and three-dimensional (3-D) cubic (Q) systems [9]. It should be noticed that all of the observed mesophases show a disordered arrangement of the hydrocarbon chains (the so-called α-conformation), as indicated by the diffuse band detected at about $(4\,\text{Å})^{-1}$ in the high-angle X-ray diffraction region [10].

The lamellar and hexagonal phases are optically birefringent and are characterized by typical X-ray diffraction patterns with sharp low angle Bragg reflections whose spacing ratios are $1:2:3:4\ldots$ and $1:\sqrt{3}:\sqrt{4}:\sqrt{7}:\sqrt{9}\ldots$, respectively [9, 10]. In the lamellar phase, the lipid molecules are associated in layers separated by water, while in the hexagonal phase, the structural elements are rods, infinitely long, all identical, crystallographically equivalent and packed in a 2-D hexagonal lattice (see figure 2). By contrast, cubic phases are optically isotropic. To-date, at least six different cubic phases have been identified and characterized [11, 12]. Their identification is based on the analysis of the spacing ratios of reflections observed in the X-ray low angle diffraction profile: the extinction symbol defines the cubic aspect of the phase and then the crystalline lattice and the symmetry of the structure [9, 11]. It should also be noted that in the hexagonal and cubic phases, a topological distinction between the inner and the outer parts of the structural elements could be made [10–13]. Therefore, two chemically distinct topologies for the molecular distribution must be considered: in one (structures of type I, 'direct'), the structural elements are filled by the paraffin chains and are embedded in the water matrix; in the other (structures of type II, 'inverted') the distribution is reversed. In both cases, the polar head groups of the amphiphile lie on the polar/apolar interface.

The data analyses for two representative compounds **1** and **9** are reported in table 1. At high dilution, corresponding to the isotropic texture I observed by optical microscopy, only a diffuse and weak band is detected in the X-ray low angle profile for all the compounds investigated. By contrast, at concentrations higher than about 0·25 (0·35 for compound **7**), strong and narrow

Table 1. X-ray diffraction data analysis: indexing of some of the experimental patterns observed for compounds **1** and **9** with different concentrations at 25°C. In the first line of the two sections of the table, the concentration c (w/w) of the acylcarnitine ester is reported. In the second line, together with the label of the identified structure, the corresponding unit cell dimensions a are indicated. s_{obs} are the reciprocal spacings in $Å^{-1}$ ($s = 2 \sin \theta/\lambda$, where 2θ is the scattering angle) of the observed reflections, while s_{lam}, s_{hex} and s_{cub} are the corresponding values calculated for 1-D lamellar, 2-D p6m hexagonal and 3-D body-centred Ia3d cubic lattices, respectively [9, 10, 11]. The following equations have been used: $s_{lam} = h/a$, $s_{hex} = (1/a)\ (2/\sqrt{3})\ (h^2 + k^2 - hk)^{-1/2}$ and $s_{cub} = (1/a)\ (h^2 + k^2 + l^2)^{-1/2}$, where h, k and l are the Miller indices of the reflections. Other notations and symbols are as in the text.

Compound 1

$c = 0{\cdot}40$ H $a = 50{\cdot}2$ Å			$c = 0{\cdot}53$ H $a = 46{\cdot}3$ Å			$c = 0{\cdot}60$ H $a = 43{\cdot}7$ Å			$c = 0{\cdot}72$ Q^{230} $a = 84{\cdot}5$ Å			$c = 0{\cdot}80$ Q^{230} $a = 82{\cdot}7$ Å			$c = 0{\cdot}90$ L_α $a = 30{\cdot}6$ Å			$c = 1$ L_α $a = 28{\cdot}1$ Å		
h,k	s_{obs}	s_{hex}	h,k	s_{obs}	s_{hex}	h,k	s_{obs}	s_{hex}	h,k,l	s_{obs}	s_{cub}	h,k,l	s_{obs}	s_{cub}	h	s_{obs}	s_{lam}	h	s_{obs}	s_{lam}
1,0	0·023	0·023	1,0	0·025	0·025	1,0	0·026	0·026	2,1,1	0·029	0·029	2,1,1	0·029	0·030	1	0·032	0·033	1	0·035	0·035
2,1	0·039	0·040	2,1	0·043	0·043	2,1	0·046	0·046	2,2,0	0·033	0·033	2,2,0	0·035	0·034	2	0·065	0·065	2	0·070	0·071
2,0	0·045	0·046	2,0	0·049	0·050	2,0	0·053	0·053	3,2,1	0·043	0·044	3,2,1	0·045	0·045						
3,1	0·062	0·061	3,1	0·066	0·066	3,1	0·069	0·070	4,0,0	—	0·047	4,0,0	0·047	0·048						
3,0	0·069	0·069	3,0	0·076	0·075	3,0	0·080	0·079	4,2,0	0·053	0·053	4,2,0	0·054	0·054						
									3,3,2	0·055	0·056	3,3,2	0·056	0·057						
									4,2,2	0·059	0·058									

Compound 9

$c = 0{\cdot}25$ L_α $a = 86{\cdot}5$ Å			$c = 0{\cdot}30$ L_α $a = 68{\cdot}1$ Å			$c = 0{\cdot}41$ L_α $a = 57{\cdot}0$ Å			$c = 0{\cdot}52$ L_α $a = 47{\cdot}5$ Å			$c = 0{\cdot}64$ L_α $a = 42{\cdot}1$ Å			$c = 0{\cdot}79$ L_α $a = 34{\cdot}5$ Å			$c = 1$ L_α $a = 35{\cdot}8$ Å		
h	s_{obs}	s_{lam}	h	s_{obs}	s_{lam}	h	s_{obs}	s_{lam}	h	s_{obs}	s_{lam}	h	s_{obs}	s_{lam}	h	s_{obs}	s_{lam}	h	s_{obs}	s_{lam}
1	0·013	0·011	1	0·014	0·014	1	0·017	0·017	1	0·021	0·021	1	0·024	0·023	1	0·026	0·028	1	0·027	0·027
2	0·026	0·023	2	0·029	0·029	2	0·035	0·035	2	0·041	0·042	2	0·047	0·047	2	0·061	0·057	2	0·055	0·055
															3	0·080	0·086			

Bragg reflections appear in this region. For compounds **4**, **7** and **9**, the observed peaks can be indexed by considering a 1-D lamellar lattice [9, 10]: therefore it appears that a lamellar L_α phase forms directly from the isotropic phase. In the case of compounds **1**, **5** and **6** the peak positions (seven Bragg peaks are observed in the best cases) are in the ratios expected for a 2-D hexagonal lattice of p6m symmetry [9, 10].

By increasing the concentration, further phase transitions are observed for compounds **1**, **5** and **6**. In particular, the X-ray diffraction low angle profile for compound **1**, at concentrations ranging from 0·6 to 0·9, is composed of several narrow Bragg peaks. In accordance with the second isotropic region (I′) observed by optical microscopy, the spacing ratios of the diffraction peaks in the order $\sqrt{6}:\sqrt{8}:\sqrt{14}:\sqrt{16}:\sqrt{20}:\sqrt{22}\ldots$ indicate the presence of a cubic structure of Ia3d symmetry [9, 11]. This phase (Q^{230} in the notation of [11]) is bicontinuous [11, 12] and its structure is now well known and accepted [11, 14, 15]: it consists of a pair of 3-D disjoined labyrinths, related to each other by an inversion centre and separated by a septum (see figure 2). It should be observed that the phase Q^{230} is known to display both type I and II topologies, depending on the chemical nature of the lipid [11, 12]. By further dehydrating compound **1**, the X-ray diffraction low angle region shows the characteristic pattern of a 1-D lamellar lattice. As the high angle region is still characterized by the diffuse band corresponding to the disordered short range conformation of the hydrocarbon chains, this phase can be indexed as L_α.

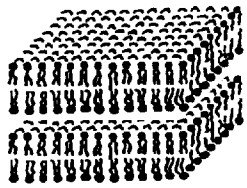

Lamellar Lα phase

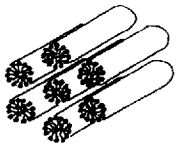

Hexagonal H phase

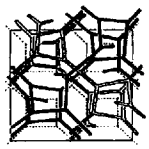

Cubic Q^{230} phase

Figure 2. Schematic representation of the structures discussed in the text. Lamellar L_α phase: the structure is formed by stacked lamellae. Each lamella is filled by the paraffin chains in the disordered α conformation (represented by short wavy lines) and is covered on both sides by the hydrophilic groups (represented by closed circles) of the amphiphile molecules. The lamellae are parallel and equidistant, without any correlation in position and orientation. Hexagonal phase: the structure is represented by parallel rods packed in a 2-D hexagonal array (space group p6m [9]). In the systems studied, the structure is of type I: the cylinders are filled by the paraffin chains and embedded in a polar matrix. Cubic Q^{230} phase: the content of the unit cell (defined by light lines) is shown in perspective. The structure, represented by a skeleton of rods, consists of two 3-D networks of rods (black and white, respectively) mutually intertwined and unconnected [11, 14, 15]. The rods are joined coplanarly 3 by 3 and occupy positions g, of symmetry 2; the rod junctions occupy positions b of symmetry 32 [9]. In the systems studied, the structure is of type I: the rods are filled by the hydrocarbon chains and are embedded in a polar matrix.

This same phase sequence follows from the optical microscopy observations for compounds **5** and **6**. According to the above proposed phase sequence, at concentrations higher than about 0·8, the X-ray diffraction profiles for both compounds show the pattern characteristic of the lamellar L_α phase. However, despite the presence of the isotropic texture I′, between the hexagonal and the lamellar phases the cubic Q^{230} phase has not been resolved for compounds **5** and **6**: probably due to metastable effects within the hexagonal and cubic structures (see, for example, [16, 17]), in this part of the phase diagram (*c* ranging from 0·6 to 0·8), the X-ray diffraction data show that at least two phases coexist in equilibrium.

In addition, it should be observed that a gel phase has been detected for compounds **5** and **6** at concentrations higher than about 0·95.

The final phase sequences are reported in table 2. In conclusion, the following two general behaviours can be envisaged: (i) compounds **1**, **2**, **5** and **6** are characterized by the most rich polymorphism, which includes hexagonal, cubic Q^{230} and lamellar L_α phases, while (ii) compounds **3**, **4**, **7–9** display only the lamellar L_α phase. In order to have a better insight into these behaviours, the concentration–temperature dependent phase diagrams for compounds **1**, **4–7** and **9** have been derived by performing X-ray diffraction experiments as a function of concentration and temperature. As the results obtained for compounds **1**, **5** and **6** on the one hand and those obtained for **4**, **7** and **9** on the other are very similar, phase diagrams relating only to the representative samples **1** and **9** are reported in figure 3. It is interesting to observe that, excluding the Q^{230}/L_α phase transition, phase boundaries are close to vertical, indicating that composition tends to be the most important factor in inducing transitions: this behaviour is generally observed for single-chain ionic amphiphiles, while for non-ionic or zwitterionic double chain systems, such as phospholipids, temperature is the most important variable, and many of the phase boundaries appear to be close to horizontal [13].

Table 2. Sequences of phases observed for the acylcarnitine esters **1**–**9**. The transition concentrations c (w/w) obtained by X-ray diffraction experiments are reported in brackets. Stars indicate those samples where the cubic phase has been detected as a single phase only by optical microscopy (see text): the reported concentrations then correspond to the limits of the coexistence region detected by X-ray diffraction.

Compound	Phase transitions
1	I —(0·20)— H —(0·60)— Q^{230} —(0·85)— L_α
2	I — H — Q^{230} — L_α
3	I — L_α
4	I —(0·30)— L_α
5*	I —(0·25)— H —(0·60)— Q^{230} —(0·80)— L_α —(0·95)— Gel
6*	I —(0·20)— H —(0·60)— Q^{230} —(0·80)— L_α —(0·95)— Gel
7	I —(0·35)— L_α
8	I — L_α
9	I —(0·20)— L_α

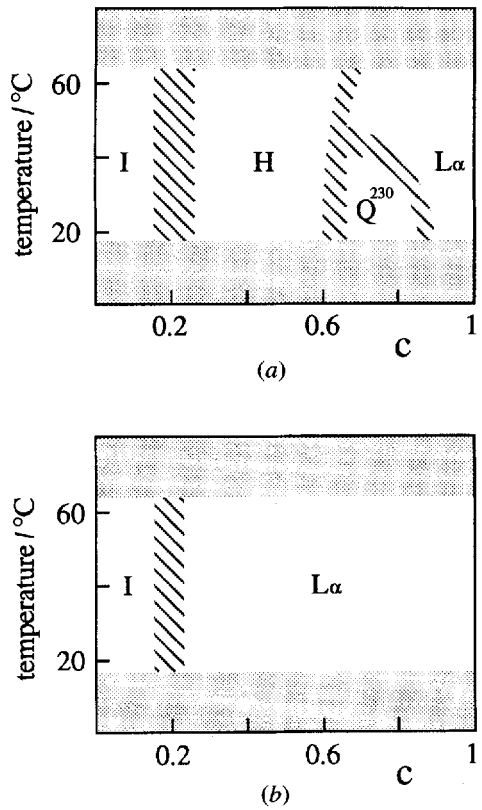

Figure 3. Representation of the temperature-concentration dependent phase diagrams of compounds (*a*) **1** and (*b*) **9**. I isotropic, H hexagonal, Q^{230} cubic and L_α lamellar phases. Hatched regions: phase coexistence. The dotted areas have not been investigated. Phase boundaries are only approximate: data points (not shown) were taken at 20, 25, 30, 40, 50 and 60°C from samples prepared at concentrations ranging from 0 to 1 with intervals of about 0·1.

3.3. *X-ray diffraction analysis: structural properties*

The unit cell dimensions of the different structures have been analysed as a function of concentration and temperature. Figure 4 shows the values obtained at 25 and 60°C for compounds **1** and **9**, and figure 5 those obtained at 25°C for compounds **4**–**7**. From the unit cell dimension and easily accessible chemical data (such as molecular weight, specific volumes and concentrations), it is possible to derive for the different phases the dimensions of the structural elements and the surface occupied by one hydrophilic head group (the area per molecule S) at the polar/apolar interface [10–12, 17]. As usual, it is assumed (i) that water is completely excluded from the paraffinic regions, (ii) that the phase composition is equal to the sample composition and (iii) that the shape of the structural elements has symmetry equal to or higher than that permitted from the space group. The analysis of these parameters is particularly important for the structures where type I and type II topologies are possible. In fact, only when the correct topology is assumed, do these parameters show reasonable values. In particular, the dimensions of the structural elements should be consistent with the volumes occupied by the polar and apolar moieties, i.e. the distance from any point in the hydrocarbon regions to the polar/apolar interface cannot exceed the length of the fully extended hydrocarbon chains. Moreover, the area per molecule at the polar/apolar interface is expected to increase (or at least not to decrease) as temperature and water content increase, even if phase boundaries are crossed [10].

The variations with concentration of the structural element dimensions and of the area per molecule at the polar/apolar interface determined for compounds **1** and **9** at 25°C and 60°C are reported in figures 6 and 7. The expressions used for the calculations are reported in the Appendix. The analysis of the thickness of the paraffinic leaflet for compound **9** (see figure 7, lower frame) indicates that no point in the paraffinic region is further from the polar/apolar interface than the fully extended length of the hydrocarbon chains (approximately 16·7 Å, as measured from molecular models). The corresponding areas per molecule at the polar/apolar interface (see

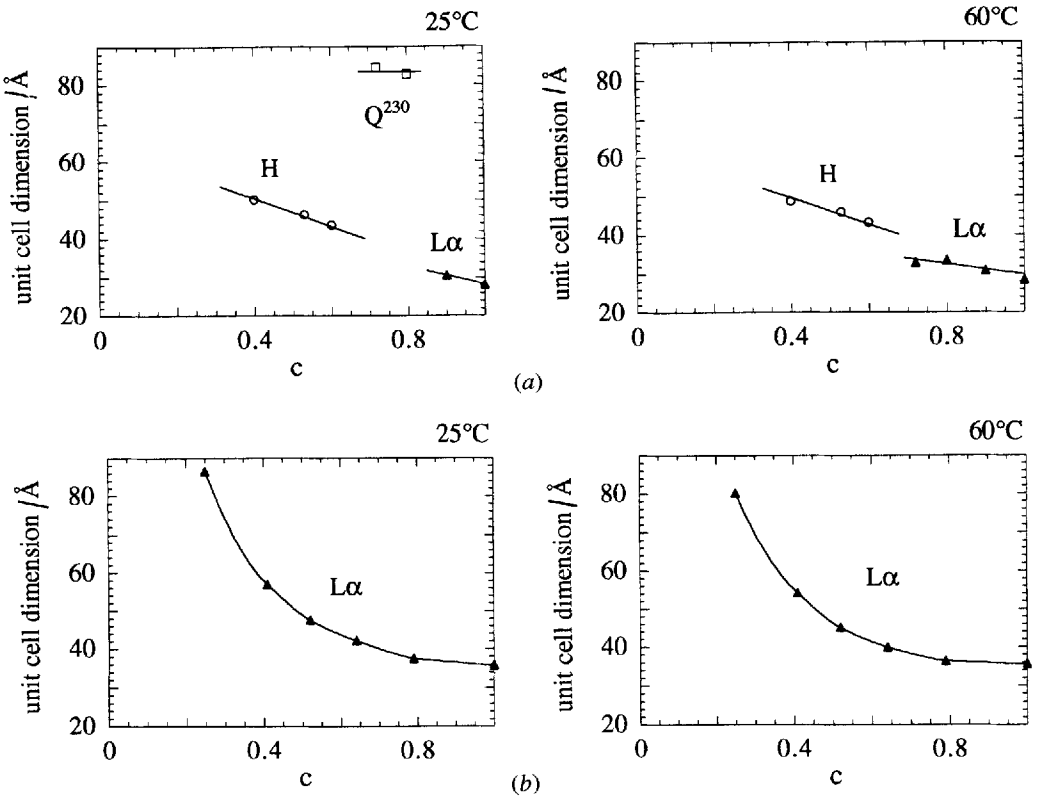

Figure 4. Variation of the unit cell dimension of the different phases for compounds (*a*) **1** and (*b*) **9** as a function of the concentration *c* at 25°C (left hand frames) and at 60°C (right hand frames). The lines are guides to the eye to show the general trends. Other symbols are as in the text.

figure 7, upper frame) are in excellent agreement with those reported for other amphiphilic systems (see, for example, [10, 11, 13]). Moreover, as expected, the areas per molecule appear to increase smoothly as the water content increases.

In the case of compound **1**, as hexagonal and cubic Q^{230} phases exist, the radii of the cylindrical structural elements and the areas per molecule have been determined assuming both type I and type II topologies (see the Appendix): the results are reported in figure 6. The behaviour observed for the radii is classical, i.e. the radius of a cylinder assumed to be of type I decreases smoothly as a function of water content, whereas the opposite occurs if the structure is supposed to be of type II [10]. The areas per molecule determined assuming a type I topology appear rather constant, also in correspondence with the phase transitions, and comparable to the values observed for compound **9**. By contrast, the area per molecule increases dramatically, giving unreasonably large values, if type II topology is assumed. Therefore, the structures of the hexagonal and cubic Q^{230} phases are deduced to be of type I. It could be observed that under this condition the calculated cylinder radii are shorter than the fully extended length of the hydrocarbon chains (approximately 15·4 Å, as measured from molecular models).

The same conclusions arise from the analysis of the data relating to the other compounds which show non-lamellar phases. Nevertheless, it should be noticed that the sequence of phases (I–H–Q^{230}–L_α) observed for these compounds is the one considered to be 'natural' for type I structures [13], so that the location of the cubic Q^{230} phase is by itself strong evidence in favour of direct structures.

4. Discussion

Inspection of the data reported above shows that the acylcarnitine esters investigated exhibit different aggregation properties. Two different phase sequence patterns have in fact been observed. Compounds **3**, **4**, **7**–**9** exhibit only one mesophase that was identified as L_α. On the other hand, compounds **1**, **2**, **5** and **6** show two more mesophases, intermediate between the isotropic solution and the lamellar phase: a hexagonal and a cubic Q^{230} phase. The analysis of the variation of the area per molecule at the polar/apolar interface as a function of concentration has indicated that the observed non-lamellar phases have

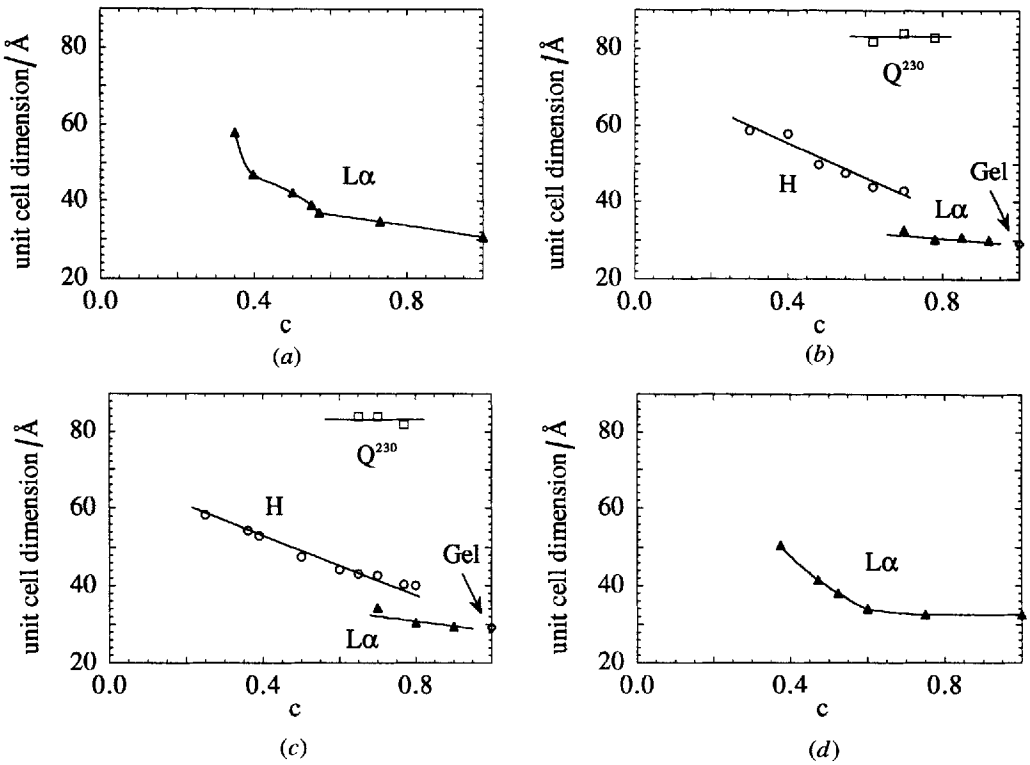

Figure 5. Variation of the unit cell dimension of the different phases for compounds **4**–**7** (*a*)–(*d*), respectively, as a function of concentration *c* at 25°C. The lines are guides to the eye to show the general trends. Other symbols are as in the text.

a type I topology. It should also be observed that micelles have been detected in the isotropic phases of compounds **1**–**6**, while multi-lamellar or uni-lamellar vesicles exist in the diluted solutions of compounds **7**–**9** [18].

The driving force behind amphiphile aggregation is the hydrophobic effect, which ensures a segregation of hydrocarbon chains away from contact with water [8, 19–21]. However, the requirement that the polar groups be hydrated forces the system to form aggregates in which all the head groups are in contact with water. It appears that the lateral stress distribution (pressure and tensions) across the lipid layer influences the self-assembly properties of amphiphile molecules [13]. Lateral stresses arise (i) from the hydrocarbon chain region (repulsive lateral pressure), (ii) from the polar/apolar interface (interfacial tension, which tends to minimize the interfacial area in order to avoid hydrocarbon–water contact) and (iii) from the head group region (lateral pressure, usually repulsive, arising from steric, hydrational and electrostatic effects). It is interesting to observe that the chain lateral pressure is strongly related to the area per molecule at the polar/apolar interface: small areas per molecule correspond to lateral pressure concentrated in the chain region, while large relative values correspond to lateral pressure mainly concentrated in the head groups. The concept of 'relative bulkiness' of the polar and apolar moieties has been introduced to appreciate qualitatively the relationships between the distribution of the lateral stresses—in the form of the amphiphile molecular shape—and the macroscopic structure of the aggregates [8, 10, 12, 13, 22, 23]; lipids preferring bilayers are roughly cylindrical, whereas molecules preferring inverted type II structures (negative polar/apolar interface) are cone-shaped, with the head group at the smaller end of the cone. Moreover, single chain lipids prefer to be organized in direct micelles or to form type I structures (positive polar/apolar interface), because these molecules have their head groups at the wide end of the cone.

As the acylcarnitine esters investigated all have the same polar head group, it is obvious that the lyotropic properties have to be related to the different structures of the hydrocarbon chains. In particular, the hexagonal and cubic phases are present in those compounds which bear a relatively short alkyl chain, *R*, of 4 or fewer carbon atoms (compounds **1**, **2**, **5** and **6**). These compounds behave as single chain surfactants, forming direct micelles at low concentration [18] and giving rise to type I non-lamellar phases at high concentrations. Derivatives bearing a relatively long alkyl chain *R* of 6 or more carbon atoms (**4**, **7**–**9**) are effective double chain surfactants and then form only the lamellar phase. Compound **3**, possessing a short alkyl chain *R*, exhibits only the lamellar phase and

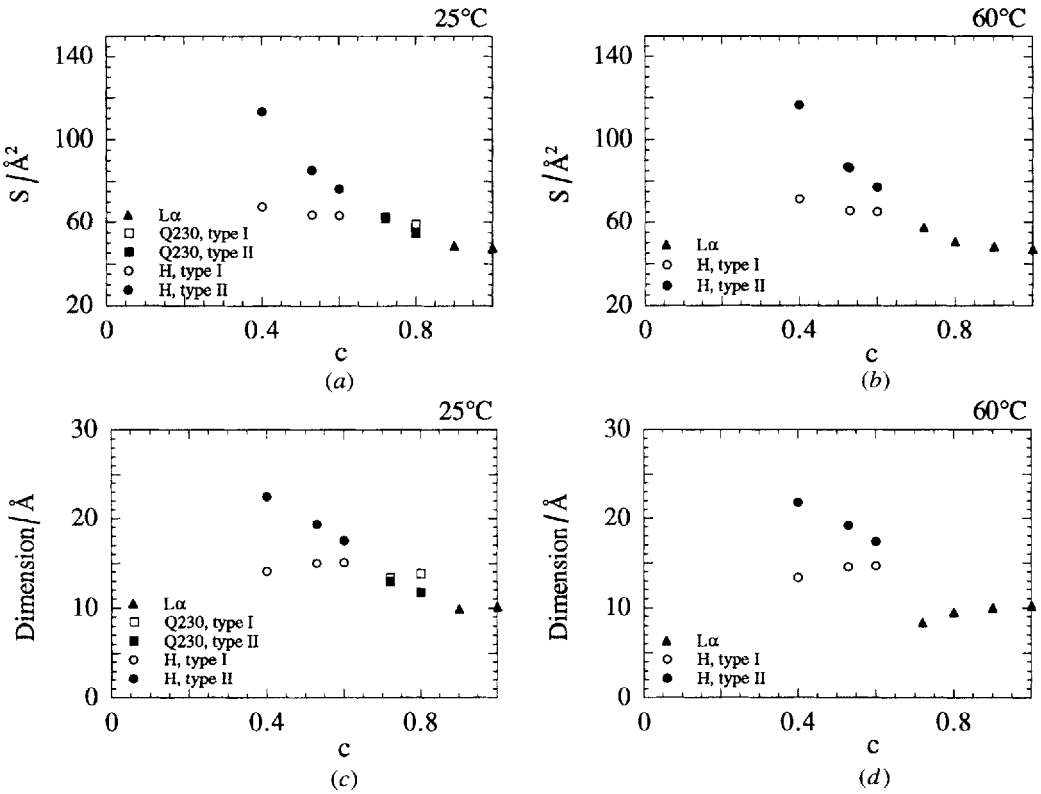

Figure 6. Dimensions of the structural elements of the different phases observed in compound **1** at 25°C (left hand frames) and 60°C (right hand frames) as a function of concentration c. Upper frames: average surface areas *per* hydrophilic group at the polar/apolar interface. Lower frames: thickness of half paraffinic leaflet in the lamellar L_α and the radius of the rods in the hexagonal H and cubic Q^{230} phases. Excluding the lamellar phase, these dimensions have been calculated considering both type I (open symbols) and type II (filled symbols) topologies (see text).

should be considered the one exception among the compounds investigated. However, in this particular case, R' is a secondary alkyl group; consequently **3** could well share a common behaviour with the effective double chain surfactants (**4**, **7**–**9**). It should be noticed finally that in this group, sample **4** is the only one yet able to form micelles in dilute solution [18].

This pictorial description can be accounted for by comparing the areas per molecule at the polar/apolar interface for the different compounds. The linear fittings throughout the experimental data obtained at 25°C are reported in figure 8. The straight lines for the compounds **1**, **5** and **6**, which appear very close to each other, show, at any concentration, larger values than those observed for compounds **7** and **9** (also very close to each other). The unique behaviour observed in the case of compound **4** is noticeable: the best-fit line falls very rapidly as the concentration increases, so that it crosses both groups of lines. These data can be directly related to the tendency of the compounds investigated to form different mesophases. For compounds **1**, **5** and **6**, the areas per molecule are relatively large, so that the interfacial tension appears to be balanced predominantly by the lateral pressure in the head group region. Therefore, the lipid layer bends towards the chains adopting a positive curvature: a normal micellar [18] and non-lamellar type I phases are observed at low concentrations in the phase diagrams. According to the concept of 'relative bulkiness', in these compounds the paraffinic to molecular volume ratio (V_{par}/V_{mol}) is relatively low (see figure 9).

By contrast, for compounds **7** and **9** we observe a reduction of the area per molecule at the polar/apolar interface, in agreement with the larger paraffinic to molecular volume ratio observed (see again figure 9). This indicates that the lateral pressure in the hydrocarbon chain region increases relatively. Therefore, the interfacial tension appears to be internally balanced by lateral pressures both in the head group and in the hydrocarbon chain region, so that the tendency of the polar/apolar interface to assume a positive curvature is strongly reduced. Only the lamellar phase is then observed in the phase diagrams. Alternatively, the internal stresses, reduced by the increased lateral pressure in the hydrocarbon chain region, are balanced across the whole bilayer: the two halves of the bilayer counteract each other since they are oppositely oriented back to back [13].

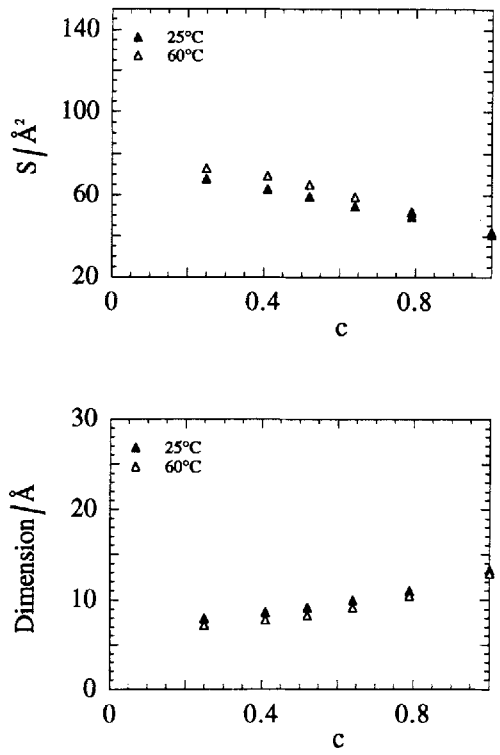

Figure 7. Dimensions of the structural elements of the lamellar L_α phase observed in compound **9** at 25°C (filled symbols) and 60°C (open symbols) as a function of concentration *c*. Upper frame: average surface areas *per* hydrophilic group at the polar/apolar interface. Lower frame: thickness of half paraffinic leaflet.

Compound **4** shows intermediate properties, as it forms direct micelles [18] followed by a lamellar phase at higher concentrations. The strong dependence of the area per molecule on concentration seems to justify this behaviour. As the concentration increases, the lateral pressure in the hydrocarbon chain region strongly increases and the tendency to form a curved interface decreases accordingly: the bilayer planar configuration appears to be the most stable at the transition to lyotropic phases.

Following the previous section, simple relationships exist between the areas per molecule at the polar/apolar interface, the paraffinic to molecular volume ratio and the phase behaviour for the compounds investigated. In order to illustrate these relationships, and to account for the peculiar behaviour of compound **4**, the notion of 'relative bulkiness' could be extended to the two alkyl chains *R* and *R'*. In particular, in figure 9, the V_{par}/V_{mol} values for the different compounds are reported as a function of the ratio of the volume of the hydrocarbon chain *R* to the volume of the total paraffinic moiety, V_R/V_{par}. Compounds which exhibit type I non-lamellar phases show low paraffinic volume ratios and low V_R/V_{par} values. When the paraffinic volume ratio increases at constant V_R/V_{par} value, the tendency to show type I non-lamellar structures disappears. The same effect is observed by increasing the V_R/V_{par} values at constant paraffinic to molecular volume ratio. In this framework, the anomalous behaviour observed for compound **4** seems to be due to its peculiar chemical structure: a low paraffinic volume ratio (which contributes to the tendency to form a positive curved

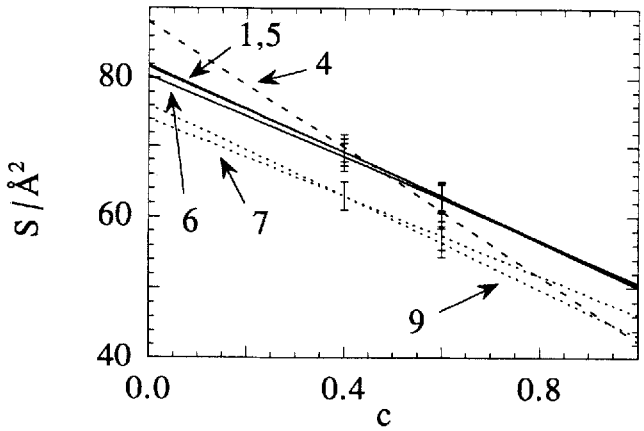

Figure 8. Best fit straight lines over all the average surface areas *per* hydrophilic group at the polar/apolar interface determined for the different compounds at 25°C. Hexagonal and cubic Q^{230} phases have been considered to have the type I topology. Continuous and dotted lines refer to compounds characterized by the I–H–Q^{230}–L_α and I–L_α phase sequences, respectively. The hatched line relates to compound **4**.

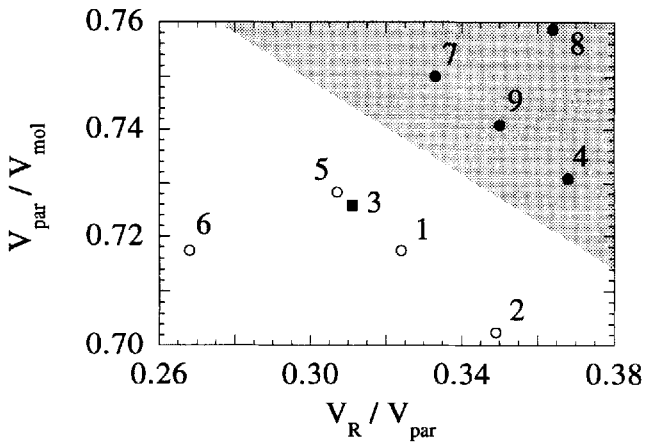

Figure 9. Schematic diagram showing the 'relative bulkiness' of the polar and apolar moieties and of the two hydrocarbon chains *R* and *R'* in the acylcarnitine ester series investigated. Abscissa: ratio of the volume of the hydrocarbon chain *R* to the volume of the paraffinic moiety (V_R/V_{par}); ordinate: paraffinic to molecular volume concentration (V_{par}/V_{mol}). Open and filled circles refer to compounds characterized by the I–H–Q^{230}–L_α and I–L_α phase sequences, respectively. The diagram has been divided into two approximative areas (white and shaded), where a homogeneous polymorphic behaviour has been observed.

interface) is in fact coupled with a large V_R/V_{par} value (which tends to stabilize a lamellar phase). It is not surprising that the final balance between these two opposite contributions is strongly dependent on concentration.

5. Conclusions

The lyotropic polymorphism of a series of alkyl esters of acyl-L-carnitine has been demonstrated. The different abilities of the compounds to form type I non-lamellar phases have been analysed by considering the areas per molecule at the polar/apolar interface and then related to the structural characteristics of the acylcarnitine molecules (i.e. the relative bulkiness of the polar and apolar moieties and of the two alkyl chains). Curved, positive interfaces (in type I non-lamellar phases) are possible only for the most polar, 'single' chain amphiphiles (**1**, **2**, **5** and **6**); the most paraffinic, 'double' chain derivatives (**3**, **7**–**9**) may generate only quasi-planar interfaces, hence exhibiting only lamellar structures. The behaviour of **4** reflects the intermediate characteristics of this particular compound.

This work was partly financed by MURST and CNR (Italy).

Appendix

For a lamellar phase, the thickness of the paraffinic layer (d_{par}) and the area per molecule at the polar/apolar interface (S) are [10] $d_{par} = ac_{v,par}$ and $S = (2V_{mol})/(ac_{v,mol})$ where a is the unit cell parameter, $c_{v,mol}$ and $c_{v,par}$ are the volume concentrations of the amphiphilic molecule and of the hydrocarbon media, respectively, and V_{mol} is the volume of the amphiphilic molecule (in Å^3).

As reported above, hexagonal and cubic Q^{230} phases could display both type I or type II structures. Therefore, knowing the cell parameter a, and assuming that the structural elements are circular cylinders (infinite in length in the case of the hexagonal and finite in length in the case of the cubic phase), the radius of the cylinder R and the area per molecule at the polar/apolar interface can be determined assuming both topologies. For the hexagonal phase, if the structure is of type I, the equations involved are [10]

$$R_I = \left(\frac{\sigma c_{v,par}}{\pi}\right)^{1/2}$$

and

$$S_I = \frac{2\pi R_I V_{mol}}{\sigma c_{v,mol}}$$

and, if the structure is of type II

$$R_{II} = \left(\frac{\sigma(1-c_{v,par})}{\pi}\right)^{1/2}$$

and

$$S_{II} = \frac{2\pi R_{II} V_{mol}}{\sigma c_{v,mol}}$$

In these equations, σ is the hexagonal unit cell surface defined as $\sigma = a^2 3^{1/2}/2$ and the indices I or II refer to the assumed topology of the structure.

For the cubic Q^{230} phase, simple geometrical calculations give the volume (V_{rod}) and the surface area (S_{rod}) of each rod [11, 17]: $V_{rod} = \pi R^2 L(1 - k_v R/L)$ and $S_{rod} = 2\pi RL(1 - k_s R/L)$ where L is the length of the rod (defined as $L = a/8^{1/2}$), and k_v and k_s are constants defined by geometrical constraints ($k_v = 0{\cdot}491$ and $k_s = 0{\cdot}735$) [17]. If the structure is type I, the volume of each paraffinic rod can be determined also by using $V_{rod,I} = (a^3 c_{v,par})/24$. Therefore, the radius R_I can be easily determined by comparing the two volumes V_{rod} and $V_{rod,I}$. The area per molecule at the polar/apolar interface is obtained by $S_I = (S_{rod}/V_{rod})V_{par}$. In the case of a structure of type II, the volume of each polar rod becomes $V_{rod,II} = (a^3 c_{v,pol})/24$, which permits us to calculate, by comparison with V_{rod}, the corresponding radius R_{II}. The area per molecule at the polar/apolar interface is

$$S_{II} = \frac{S_{rod}}{V_{rod}}\left(V_{pol} + \frac{1 - c_{mol}}{c_{mol}}\frac{M_{mol}}{M_{wat}}V_{wat}\right)$$

where c_{mol} is the amphiphile weight concentration, V_{wat} is the volume of a water molecule (29·9 Å^3) and M_{mol} and M_{wat} are the corresponding molecular weights.

References

[1] Bremer, J., 1983, *Physiol. Rev.*, **63,** 1420.
[2] Murthy, M. S. R., and Pande, S. V., 1984, *J. Biol. Chem.*, **259,** 9082.
[3] Stinson, R. H., 1990, *Chem. Phys. Lipids*, **52,** 29.
[4] Pande, S. V., 1981, *Biochim. Biophys. Acta*, **663,** 669.
[5] De Maria, P., Fontana, A., Frascari, S., Gargaro, G., Spinelli, D., and Tinti, M. O., 1994, *J. Pharm. Sci.*, **83,** 742.
[6] Bohmer, T., and Bremer, J., 1968, *Biophys. Acta*, **152,** 569.
[7] Tardieu, A., 1972, Ph.D. thesis, Université Paris-Sud.
[8] Tanford, C., 1980, *The Hydrophobic Effect: Formation of Micelles and Biological Membranes*, 2nd edition (John Wiley).
[9] *International Tables for X-ray Crystallography*, 1952 (The Kynoch Press).
[10] Luzzati, V., 1968, *Biological Membranes*, Vol. 1, edited by D. Chapman (Academic Press), p.71.
[11] Mariani, P., Luzzati, V., and Delacroix, H., 1988, *J. Molec. Biol.*, **204,** 165.
[12] Luzzati, V., Vargas, R., Mariani, P., Gulik, A., and Delacroix, H., 1992, *J. Molec. Biol.*, **228,** 1.
[13] Seddon, J. M., 1990, *Biochim. Biophys. Acta*, **1031,** 1.
[14] Luzzati, V., and Spegt, P. A., 1967, *Nature (London)*, **215,** 701.

[15] DELACROIX, H., GULIK-KRZYWICKI, T., MARIANI, P., and RISLER, J.-L., 1993, *Liq. Crystals*, **5,** 605.
[16] AMBROSINI, A., BERTOLI, E., MARIANI, P., TANFANI, F., WOZNIAK, M., and ZOLESE, G., 1993, *Biochim. Biophys. Acta*, **351,** 1148.
[17] GULIK, A., LUZZATI, V., DE ROSA, M., and GAMBACORTA, A., 1985, *J. Molec. Biol.*, **182,** 131.
[18] Unpublished results.
[19] ISRAELACHVILI, J. N., MITCHELL, D. J., and NINHAM, B. N., 1976, *J. chem. Soc. Faraday Trans. 2*, **72,** 1525.
[20] ISRAELACHVILI, J. N., MARCELJA, S., and HORN, R., 1980, *Q. Rev. Biophys.*, **13,** 121.
[21] MITCHELL, D. J., and NINHAM, B. W., 1981, *J. chem. Soc. Faraday Trans. 2*, **77,** 601.
[22] LUZZATI, V., and HUSSON, F., 1962, *J. Cell. Biol.*, **12,** 207.
[23] DE KRUIJFF, B., 1987, *Nature*, **329,** 587.